PHYSICAL REVIEW B VOLUME 41, NUMBER 18 15 JUNE 1990-II

Structure and evolution of the displacement field in hydrogen-implanted silicon

G. F. Cerofolini, L. Meda, and C. Volpones
Functional Materials Laboratory, EniChem, via S. Salvo 1, I-20097 San Donato MI, Italy

G. Ottaviani and J. DeFayette
Dipartimento di Fisica, Università di Modena, I-41100 Modena MO, Italy

R. Dierckx, D. Donelli,* and M. Orlandini*
EEC Joint Research Center, I-21020 Ispra VA, Italy

M. Anderle and R. Canteri
Divisione di Scienza dei Materiali, Istituto per la Ricerca Scientifica e Tecnologica (IRST), I-38050 Povo TN, Italy

C. Claeys and J. Vanhellemont
Interuniversity Micro-Electronics Center (IMEC), Kapeldreef 75, B-3030 Leuven, Belgium
(Received 27 December 1989)

Hydrogen implantation into silicon at room temperature and at 77 K has been studied by secondary-ion mass spectrometry (SIMS), elastic recoil diffusion analysis (ERDA), Rutherford backscattering spectroscopy (RBS), multiple-crystal x-ray diffraction (XRD), conventional and high-resolution transmission electron microscopy (TEM and HREM), and binary-collision simulation (MARLOWE). The implantation energy was 15.5 keV, low enough not to form dense collisional cascades; the fluence range was 10^{14} to 2×10^{16} cm^{-2}. Annealing experiments were carried out by heating the implanted samples for 2 h in the temperature interval 400–800 °C. While the hydrogen profile is well described by MARLOWE simulation, the resulting crystal deformation, measured by RBS, XRD, TEM, and HREM, cannot be interpreted in terms of damage imparted to the silicon target, but is mainly related to the displacement field around hydrogen. An accurate analysis is, however, able to separate the contributions due to self-interstitials from that due to hydrogen. The threshold energy for Frenkel-pair production is determined and is found to be 43±5 eV, remarkably higher than the commonly accepted value of 15 eV.

I. INTRODUCTION

The implantation of hydrogen into single-crystal silicon is thought to be almost a perfect experiment for studying the damage produced by recoils with low transferred energy. From one side the high crystalline quality and the purity of the electronic-grade single crystal makes silicon the favorite target for this purpose and, on the other side, the hydrogen-to-silicon mass ratio prevents the formation of dense collisional cascades, provided that hydrogen is implanted into silicon at energies in the kiloelectronvolt range. No target amorphization is expected to occur and the damage is essentially due to the formation of vacancy-interstitial Frenkel pairs (FP's). The aim of this work is to give an experimental estimation of the defect amount and distribution in the target due to hydrogen ion implantation and to compare it with the theoretical description given by damage simulation codes.

The detection of this defect distribution is, however, a difficult task, both because it is poorly known whether or not point defects created in silicon are mobile at room temperature and because each measurement of defects in a crystal is perturbed by the presence of long-range displacement fields, due to the defects themselves and (mostly) to the implanted impurity (the attribute "long" means that the displacement field extends to a relevant number of atoms and is not exhausted to nearest neighbors).

In recent years we have studied hydrogen implantation into silicon by using the following techniques: secondary-ion mass spectrometry (SIMS), Rutherford backscattering spectroscopy (RBS) in channeling, double-crystal x-ray diffraction (XRD), transmission electron microscopy (TEM), and high-resolution electron microscopy (HREM). The measurements were, however, difficult to interpret because all these techniques detect a perturbation in the crystal due not only to the presence of point defects, but also to the presence of the implanted hydrogen, which strongly perturbs the silicon lattice around it.[7]

The incorporation of hydrogen in silicon is an important area of research and many authors investigated both the produced damage and the bonding configurations of hydrogen in the silicon lattice. As knowledge of the behavior of hydrogen is a necessary prerequisite for interpretation of the experimental results, useful information from the review of Pearton *et al.*[2] is summarized below.

Hydrogen may be present in the silicon lattice in at least three forms.

(i) The configuration with the lowest potential energy is

 ©1990 The American Physical Society

hydrogen bonded to a dangling bond at a defect site (configuration referred to as Si-H); this configuration is immobile and probable up to around 500 °C.

(ii) Hydrogen forms H_2 molecules when it is present in a perfect lattice; this electrically and optically inactive configuration is thermodynamically preferred to the atomic one; H_2 occupies an interstitial site under equilibrium conditions and is immobile up to approximately 500 °C.

(iii) Hydrogen preserves the atomic configuration when the following conditions are simultaneously satisfied: low concentration, absence of defect sites, and high temperature T ($T > 500$ °C); atomic-hydrogen diffusivity is high even at room temperature.

The formation of hydrogen platelets directed along {111} planes, whose structure is still controversial, is also reported in silicon containing a high hydrogen concentration.[3]

By ion implantation, hydrogen is injected as atoms in the lattice; the above considerations suggest that this form is preserved at low fluences and in an undamaged lattice. When the hydrogen concentration increases, the atoms form molecules, and when the lattice gets more and more broken, the Si-H configuration becomes the most stable one. The above three forms tend to be in dynamic equilibrium with one another, so that at low temperature ($T < 500$ °C) the bonded forms are expected to predominate, rendering hydrogen relatively immobile, while at high temperatures the fast diffusing atomic form is expected to dominate.

In Ref. 1 it is shown that the hydrogen profiles obtained by SIMS measurements after room-temperature implantation match the ones computed by a binary-collision code,[4] thus giving evidence for the absence of long-range diffusion phenomena. We feel that hydrogen, injected into the crystal as an atomic ion, can react and transform into more stable bonded configurations (Si-H, H_2, etc.) where it stops.

Molecular hydrogen H_2 is assumed to be a stressing impurity and to be the source of a large displacement field in the silicon lattice, the energy required for the lattice distortion being furnished by the electronic energy gained in the reaction $H + H \rightarrow H_2$. The displacement field due to the impurity superimposes on the damage produced by recoils and may mask it. If this hypothesis is correct, the displacement field can be removed by annealing the samples at $T > 500$ °C, which produces H_2 dissociation and makes hydrogen mobile as single atoms. This heat treatment, however, is responsible for a lattice reconstruction so that the annealed samples are not suitable for the detection of the damage imparted to the crystal. It is therefore necessary to analyze accurately the as-implanted samples in order to separate the various contributions to the observed displacement fields.

II. EXPERIMENTAL

A. Sample preparation

Samples were prepared by implanting H_2^+ into single-crystal silicon. Silicon slices were 4 in. in diameter, Czochralski grown, (100) oriented, p type with a resistivity in the interval 30–50 Ω cm. The implantations were carried out by tilting the slices by 7° with respect to the beam.

Samples were implanted with H_2^+ at an energy of 31 keV. Because of the H_2^+ fragmentation at the surface and the low density of the collisional cascades, this implantation is equivalent to the implantation of atomic hydrogen at double fluence and energy of 15.5 keV. The results of Mitchell et al.[5] confirm this conclusion. Data will henceforth be presented in terms of atomic energy E and fluence Φ.

The implantations were carried out in an Eaton Nova 10/160 ion implanter, operated at a beam current density of approximately 1 mA/cm^2; a moderate increase of temperature during the implantation is present and estimated to be below 100 °C; this process will be referred to as carried out at room temperature in the high current mode [RT(HCM)]. These samples were often stored at room temperature for times greater than 10^3 h before analysis. Occasionally, targets were implanted in a Varian ion implanter with a suitably modified end station at very low current density (≈ 1 μA/cm^2) at 293 K (referred to as RT) or at approximately 77 K by cooling the target with liquid nitrogen (referred to as LNT). LNT samples were stored in liquid nitrogen up to their characterization; no RBS relevant changes were detected after aging at room temperature for variable durations up to 10^3 s. The fluence ranged between 10^{14} and 2×10^{16} cm^{-2}, the lower value being dictated by the sensitivities of the various experimental techniques and the upper value being dictated by the need not to modify appreciably the target composition.

Annealing experiments were carried out by heating the samples in a vacuum for 2 h in the temperature interval 400–800 °C. Data for RT(HCM) implantation at 75 keV are reported in Ref. 1; a few samples, with thickness around 100 μm, were irradiated with protons at 21 MeV to separate the effect of damage from that of hydrogen.

B. Measurements

1. Hydrogen profiles

Though nonlinear effects may influence the implanted profile,[6] we preferred to characterize hydrogen profiles obtained by high-fluence implantations. Indeed, since hydrogen in atomic form is presumably fast diffusing while in bonded forms (H_2, Si-H, etc.) it is immobile up to 400 °C, one has a better chance to "freeze" the as-implanted profile by allowing for short paths for encounters (H-H, H-vacancy, etc.) leading to an immobile form.

Secondary-ion mass spectrometry measurements were carried out by using a CAMECA IMS-4F ion microprobe with a sample chamber vacuum of about 5×10^{-7} Pa. The beam probe was formed by Cs^+ ions; the acceleration energy was 10 keV, and the primary current density was 5 mA/cm^2, stable during the measurements to within 0.5%. To minimize crater-edge effects, secondary ions were collected only from a circle with diameter 10 μm in

the central region inside the total rastered area of 500×500 μm^2. These particular conditions allow us to reduce typical problems of hydrogen depth profiling, mainly related to the contamination of the sample chamber.[7] Knock-on artifacts affect the hydrogen profiles particularly in the tails, where the hydrogen concentration is lower than 2×10^{18} cm^{-3}. This effect is responsible for an uncertainty in the depth scale smaller than 10 nm, and of a background level increase. The depth resolution is less than 10 nm.

To avoid the characterization of artifacts and of diffused profiles, we limit our considerations around the maxima of the distributions. Less sensitive elastic recoil diffusion analyses (ERDA) were used to follow the hydrogen evolution after annealing in the concentration region just above 10^{20} cm^{-3}.

2. *Displaced silicon profiles*

Channeling RBS spectra were obtained by impinging a 1-MeV He^+ beam into implanted samples, with a merging angle of 130°, and an integrated charge in the range 30–100 μC. Spectra were compared with those obtained from an undamaged reference sample both in channeling and in random conditions.

Conventional and high-resolution transmission electron microscopy investigations were performed with a JEOL 200 CX microscope (at Antwerp University). Cross-section samples were prepared by using a technique described extensively elsewhere.[8]

Multiple-crystal x-ray diffraction was employed to determine the depth distribution of the components normal to the sample surface of lattice strain ($\epsilon_\perp$) and static Debye-Waller factor. The used geometry was the conventional $(n,-n)$ parallel configuration with (400) silicon as operating reflections and CuK_{α_1} as incident wavelength. The experimental rocking curves were simulated by means of the semikinematical approximation of the dynamical theory of diffraction from imperfect crystals.[9] The best fits were obtained by varying the parameters that define the depth distribution of strain $\epsilon_\perp$ and root-mean-square (rms) *static* displacement u_0^{stat}.

C. Theoretical simulations

MARLOWE code[4] was extensively used both to simulate the hydrogen and interstitial profiles and to interpret RBS data. This code is an excellent calculation tool to simulate primary radiation damage in crystalline targets. The path of an irradiating or source particle is followed through a material by solving classical equations of motion. Underway, the particle loses energy in inelastic collisions with the electrons and collides with the nuclei. In such a collision, energy is transferred to the target nucleus. If the transferred energy is greater than the damage threshold energy, the target nucleus is ejected from its lattice site and becomes a primary knock-on atom leaving a vacancy behind. The primary knock-on atoms wander through the material and collide further with the lattice atoms, producing new knock-on atoms and vacancies. When all recoils have come to rest, a certain number of Frenkel pairs remain, grouped together in a displacement cascade. The code is used to simulate hydrogen implantation in silicon, resulting in the implanted hydrogen profile and in the profiles of self-interstitials and vacancies.

A large part (about 95%) of the energy lost by the protons is due to inelastic scattering with electrons. The electronic stopping power, which therefore plays a major role in the description of the profile, is the one compiled by Andersen and Ziegler[10] multiplied by a factor a_H in order to fit better with the experimental results.

By means of a special adapted version of MARLOWE (using a spatially compressed crystal), RBS spectra are calculated starting from an assumed interstitial profile and simulating the experimental RBS procedure with all its details (beam divergence, energy definition, detector resolution). The result so obtained has to be compared with the experimental RBS spectrum (depured from the contributions due to the unimplanted region of the crystal and due to multiply scattered He^+).

III. EXPERIMENTAL EVIDENCE AND ANALYSIS OF DATA

Unless otherwise specified, the following considerations apply to RT(HCM) samples.

A. As-implanted samples

1. *Hydrogen profiles*

The hydrogen profiles measured with SIMS in samples implanted at 15.5 keV at two fluences, 4×10^{15} and 2×10^{16} cm^{-2}, are shown in Fig. 1; they are accurately

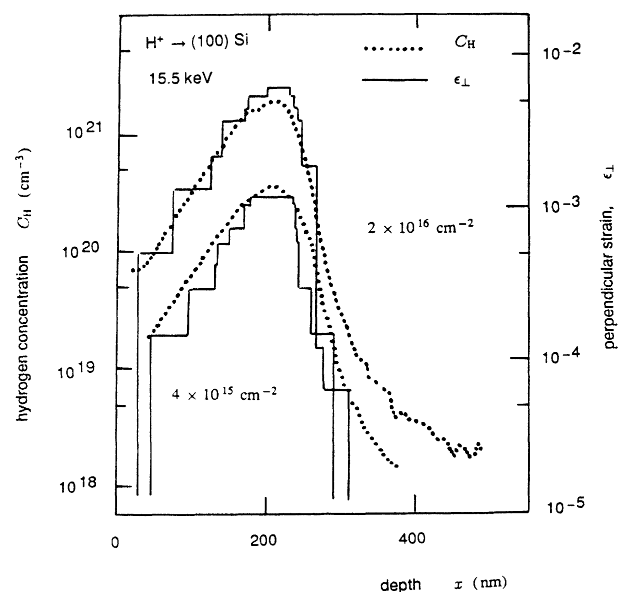

FIG. 1. Hydrogen profiles after implantation at 15.5 keV at two fluences compared with the corresponding perpendicular-strain profiles.

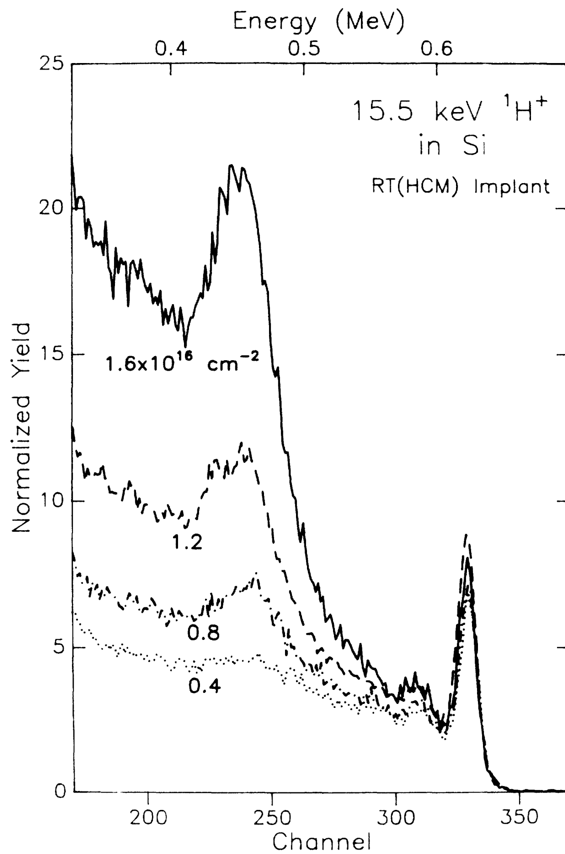

FIG. 2. RBS spectra of RT(HCM) samples implanted at 15.5 keV for several fluences in the interval $4\times10^{15}-1.6\times10^{16}$ cm^{-2}.

reproduced with MARLOWE simulations by using the multiplying factor $a_{\mathrm{H}}=1.24$. It has to be noted that the Ziegler stopping powers have an uncertainty of $\pm10\%$. Moreover, at energies below 10 keV, mainly theoretical calculations of the stopping powers are available and the few measurements differ by about 50%. The value of a_{H} seems hence reasonable and is not in contrast with the Andersen and Ziegler compilation.[10] (Hydrogen profiles in samples implanted at 75 keV gave an adequately corresponding fit with MARLOWE simulations by taking $a_{\mathrm{H}}=1.10$.)

2. *Damage profiles*

Assuming the perpendicular-strain profile to be proportional to the interstitial concentration, the calculated damage profiles and the measured XRD profiles do not coincide—calculated damage profiles lie nearer to the surface (shifted by about 40 nm) and have a relatively strong component between the surface and damage peak. Also the RBS spectra calculated from the damage profiles do not coincide with the measured RBS spectra (shown in Fig. 2).

In Table I are listed the projected ranges R_p, standard deviations σ_p, skeweness γ_1 and kurtosis γ_2 of the hydrogen, strain and displaced silicon (Si_d) profiles for the samples implanted at 15.5 keV at high and low fluence, respectively. For a comparison the same momenta for silicon interstitials (Si_i) as calculated by MARLOWE are also given. These calculations were carried out by assuming a threshold energy of 15 eV (Andersen[11] determined $E_t=14$ eV; Ziegler[12] suggests $E_t=15$ eV); however, no relevant changes in the *distribution* of interstitials are observed for threshold energy E_t in the range 15–75 eV (the total *amount* varying approximately as $E_t^{-\alpha}$, with $\alpha=1.42\pm0.04$). Within experimental uncertainties, the distributions of hydrogen concentration $C_{\mathrm{H}}(x)$, perpendicular strain $\epsilon_\perp(x)$, and displaced silicon $C_d(x)$ have the same momenta and are presumably related to one another, and not directly related to the distribution of interstitials $C_i(x)$. The defect spatial distribution, as detected by cross-section TEM [Figs. 3(a) and 3(b)], is consistent with the assumption that the extended defects too are due to hydrogen-related complexes; Fig. 3(c) shows a (111) platelet similar to the ones observed by Ponce *et al.*[3] The samples irradiated with 21-MeV protons, in which no hydrogen remains in the sample, show an RBS signal (which in principle depends on parallel strain and rms displacement, but not on perpendicular strain), while the XRD measurement does not reveal a perpendicular strain but only a static disorder.

Table I shows that the experimental distributions $C_{\mathrm{H}}(x)$, $\epsilon_\perp(x)$, and $C_d(x)$ have momenta that remain con-

TABLE I. First momenta of the distributions of hydrogen, perpendicular strain, displaced silicon, and silicon self-interstitials.

	R_p (nm)	σ_p (nm)	γ_1	γ_2	Notes
High fluence					
C_{H} (SIMS)	178±3	50	−0.68	1.17	$\Phi=2.0\times10^{16}$ cm^{-2}
$\epsilon_\perp$ (XRD)	185±2	48	−0.78	0.30	$\Phi=2.0\times10^{16}$ cm^{-2}
Si_d (RBS)	184±4	49	0.74	1.96	$\Phi=1.6\times10^{16}$ cm^{-2}
Low fluence					
C_{H} (SIMS)	181±5	53	−0.65	0.94	$\Phi=4.0\times10^{15}$ cm^{-2}
$\epsilon_\perp$ (XRD)	185±2	46	−0.76	0.35	$\Phi=4.0\times10^{15}$ cm^{-2}
Si_d (RBS)	195±5	67	0.68	0.60	$\Phi=4.0\times10^{15}$ cm^{-2}
Si_i (MARLOWE)	118±1	59	−0.26	−0.83	$E_t=15$ eV
Si_i (MARLOWE)	119±1	56	−0.20	−0.83	$E_t=40$ eV

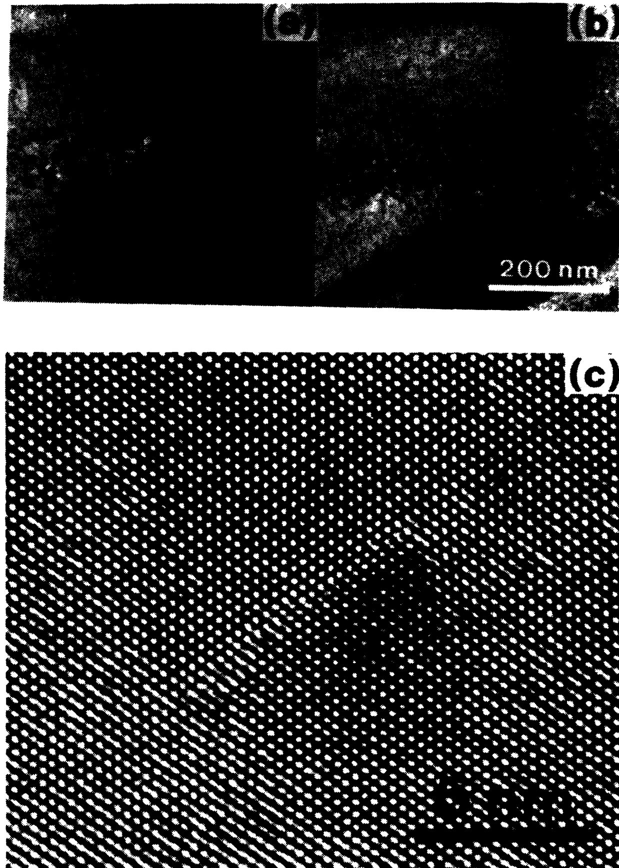

FIG. 3. (a) TEM cross section of the as-implanted RT(HCM) sample at $\Phi=4\times10^{15}$ cm^{-2}, (b) the same as (a) but with $\Phi=2\times10^{16}$ cm^{-2}, and (c) HREM image of part of sample (b) showing a (111) platelet similar to the ones observed by Ponce *et al.* (Ref. 3).

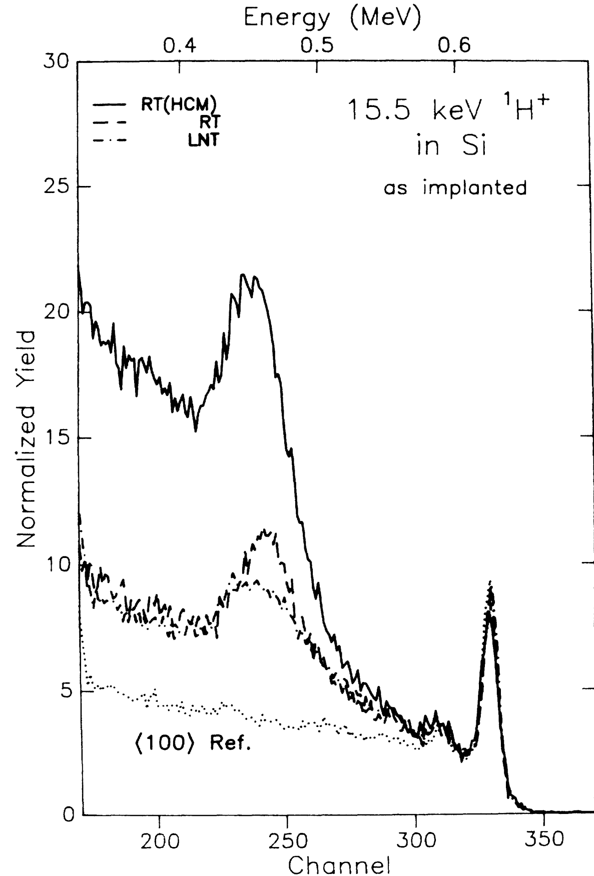

FIG. 4. Comparison of the RBS spectra of the as-implanted RT(HCM), RT, and LNT samples ($\Phi=1.6\times10^{16}$ cm^{-2}).

stant with Φ; this fact suggests that these profiles scale linearly with the implanted fluence. A finer inspection of XRD and RBS data shows, however, that (1) $\epsilon_{\perp}^{\max}$ increases with a slight superlinearity with Φ for $\Phi\gtrsim10^{15}$ cm^{-2} ($\Phi=10^{15}$ cm^{-2} corresponds to a maximum hydrogen concentration $C_{\rm H}^{\max}\simeq10^{20}$ cm^{-3});[6] (2) $u_0^{\rm stat}$ increases as $C_{\rm H}^{\beta}$, with $\beta=2.25\pm0.05$, for C_H in the range 2×10^{20}–3×10^{21} cm^{-3}, determined by the behavior of $u_0^{\rm stat}$ in the neighborhood of $C_{\rm H}^{\max}$ (obtained by the collaboration of Ref. 1, but not presented therein); and (3) the RBS spectra of samples implanted at assigned temperature and different fluences (Fig. 2) show a more-than-linear increase of the bulk peak with fluence.

In particular, the RBS spectra show that the signal has two contributions: one coming from the *subsurface region* (depth down to approximately 100 nm, where the hydrogen concentration is small), which increases in proportion to Φ (Fig. 2) and is independent of the implantation temperature and beam current density (Fig. 4), and the other coming from the *bulk region* (where hydrogen concentration is maximum), which scales more than linearly with Φ and has a paradoxical behavior versus implantation temperature (Fig. 4 and Ref. 13).

B. Annealed samples

The hydrogen profiles determined by ERDA after annealing in the temperature range 400–600 °C (Fig. 5) demonstrate that hydrogen starts to diffuse out at a temperature around 400 °C. The evolution of channeling RBS spectra (Fig. 6) demonstrates that the loss of hydrogen is responsible for an appreciable annihilation of the displacement field. The thermal treatment at 400 °C (which produces a small hydrogen loss) is responsible for a strong increase of the displacement field. These combined facts lead us to conclude that *most of the displacement field is due to the hydrogen configuration that has been formed during annealing at 400 °C.* Figure 4 also shows that the RBS spectra of the LNT, RT, and RT(HCM) samples coincide in the subsurface region (down to a depth x of approximately 100 nm, where hydrogen concentration is below 2×10^{20} cm^{-3}) and that in the bulk region the signals are scaled in the order LNT $<$ RT $\ll$ RT(HCM). This result shows that the (presumably atomic) hydrogen configuration in the LNT samples is not responsible for the observed displacement fields.

Figures 7(a) and 7(b), showing the cross-section TEM images of samples, respectively, as-implanted and annealed at 650 °C for 30 min, indicate that this annealing extends the size of as-implanted defects and decreases

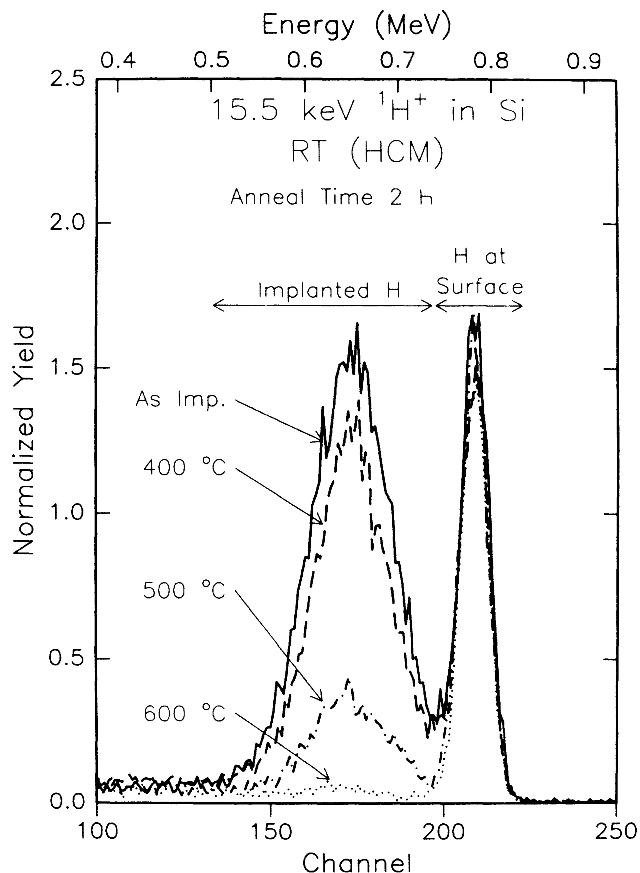

FIG. 5. Hydrogen profile evolution after 2-h annealing of RT(HCM) samples at several temperatures in the range 400–600 °C ($\Phi = 1.6\times10^{16}$ cm^{-2}).

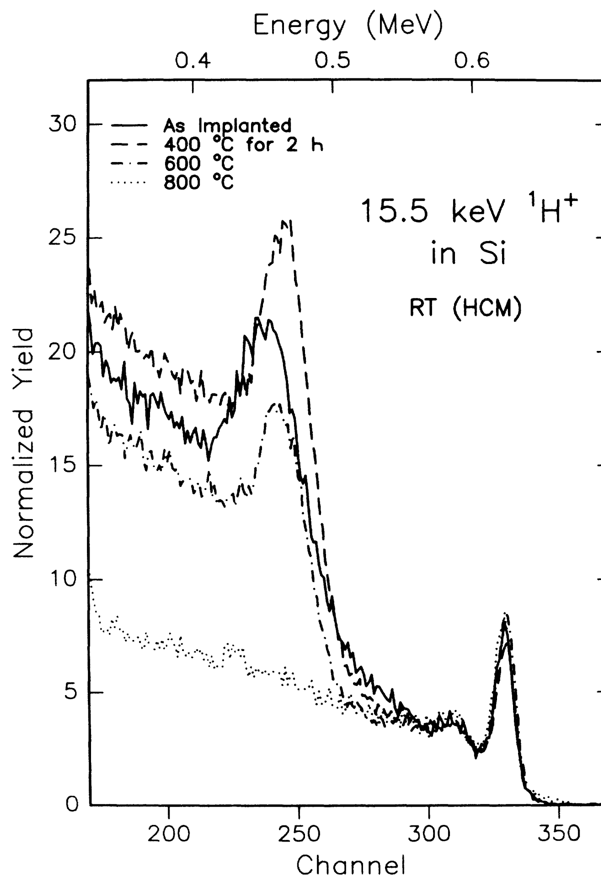

FIG. 6. RBS spectrum evolution after 2-h annealing of RT(HCM) samples at several temperatures in the range 400–800 °C ($\Phi = 1.6\times10^{16}$ cm^{-2}).

their density. Dominant defect habit planes are {113} and {001}; Fig. 7(c) shows a high-voltage electron microscope image of a (001) platelike defect. An RBS channeling analysis (not reported) at two energies, 1 and 2 MeV, shows, moreover, that the dechanneling factor does not depend on energy, thus giving evidence that the scattering centers are neither dislocations nor stacking faults.

IV. DISCUSSION

The experimental results have highlighted the following: (1) At the same implantation temperature the bulk displacement field increases with the fluence, (2) at the same fluence the bulk displacement field increases with the implantation temperature,[13] (3) there is a strong correlation between hydrogen concentration and displacement field in the bulk as shown by annealing experiments, (4) near the surface there exists a zone in which the displacement field behaves after annealing differently from the bulk, and (5) 21-MeV proton irradiations (no hydrogen present) show no strain and high disorder.

These facts, as expressed in Figs. 2, 4, 5, and 6, show that most of the observed field is produced neither by the radiation damage (this conclusion having already been reached earlier[14] as well as more recently[1,15]) nor by atomic hydrogen injected into the crystal; rather, the displacement peak is due to some other hydrogen configuration. This configuration cannot involve long-range rearrangement because the hydrogen profile in the as-implanted sample is well described by MARLOWE simulation. We assume that *the hydrogen configuration responsible for the strong displacement field is molecular hydrogen* H_2. Though there is a reasonable consensus on this point,[2] more exotic configurations or nonstoichiometric silicon-hydrogen compounds cannot be excluded; however, all the forthcoming considerations hold true irrespective of the actual hydrogen configuration.

The second assumption is based on the following considerations: The measured hydrogen and perpendicular-strain profiles are very similar and independent of the fluence (Fig. 1 and Table I). A slight superlinearity is observed for the perpendicular strain for fluences higher than 10^{15} cm^{-2} (Ref. 6); in contrast, the static rms displacement u_0^{stat} shows more than a squared dependence as a function of the hydrogen concentration or fluence.

According to a recently proposed model,[16,17] a displacement field of N_{dis} atoms ($N_{\text{dis}} \simeq 5\times10^2-10^3$) surrounds each substitutional impurity in silicon. Our second assumption is that *this property characterizes any impurity, irrespective of its lattice location.* In this hypothesis, if the displacement fields due to different impurities do not overlap, average strain and disorder grow

linearly with impurity concentration C; if they overlap (which happens for $C \gtrsim \bar{C} = n_{\rm Si}/N_{\rm dis} \simeq 5\times10^{19}$ to 10^{20} cm^{-3}, where $n_{\rm Si}$ is the silicon atomic density), nonlinear phenomena arise. While it is difficult to predict which kind of nonlinearity affects $\epsilon_\perp(C)$, in view of the open structure of the silicon lattice we expect a strong increase of the rms displacement $u_0(C)$ as soon as C exceeds $\bar{C}$. It is to be noted that the static disorder as observed by XRD, $u_0^{\rm stat}$, must be composed quadratically with the thermal disorder, $u_0^{\rm th}$, to obtain the rms displacement u_0 that is responsible for the RBS signal,

$$u_0^2 = (u_0^{\rm th})^2 + (u_0^{\rm stat})^2 \ . \tag{1}$$

As a conclusion, two zones can be identified: a subsurface zone with small hydrogen concentration, extending to around 100 nm for an implantation fluence of 10^{16} cm^{-2} (the lower the fluence, the greater the extension of the subsurface zone), and a bulk region where hydrogen concentration is maximum.

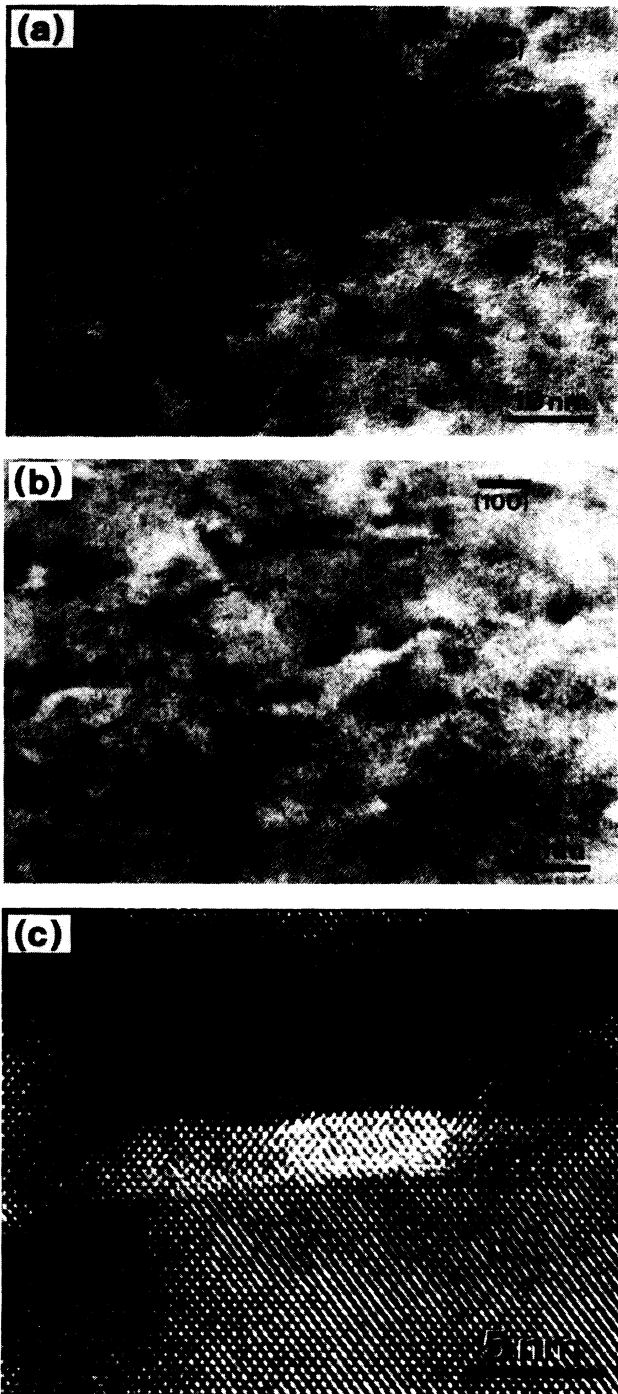

FIG. 7. (a) HREM cross section of an RT(HCM) as-implanted sample ($\Phi = 2\times10^{16}$ cm^{-2}). (b) Same sample annealed at 650 °C for 30 min. Coarsening of the defects is observed and the dominant habit planes are {113} and {001}. (c) High voltage image of a (001) platelike defect.

A. Subsurface region

The implanted zone at the depth 50–100 nm has been studied in detail. The lower limit, below which no reliable data can be extracted because of the surface peak, is imposed by experimental RBS spectra. The higher limit is related to the appearance of nonlinear effects.

In this region the following observations are noted: (1) RBS gives evidence for displaced atoms, (2) XRD shows a strain that is small or even below the detection limit and gives no indication for static disorder, (3) TEM shows the absence of extended defects, and (4) MARLOWE calculations show a non-negligible damage production (the surface concentration of interstitials is approximately 30% of the peak concentration[6]).

Taken together, these facts show that in the region where close FP's are produced (item 4), displaced atoms Si_d are present (item 1), without important long-range deformation (item 2) and without extended defects (item 3). Hence it is almost mandatory to conclude that the observed *displaced atoms are close vacancy-interstitial Frenkel pairs only, the associate displacement field being negligible*: $Si_d = Si_i$.

We assume that in the subsurface region the displacement field detected as RBS signal is purely due to directly produced FP's. Interpreting the experimental RBS data from LNT sample (implanted at 77 K) in terms of calculated interstitial distribution, the damage efficiency y (i.e., the number of FP's produced per implanted hydrogen) is obtained. The experimental RBS spectrum is reconstructed, within the uncertainty, by assuming a threshold energy given by $E_t = 43\pm5$ eV with null recombination distance (Fig. 8); from the numerical point of view, this situation is approximately equivalent to a threshold energy of 15 eV with a recombination distance of 1.2 lattice constants. The damage efficiency is $y = 2.3\pm0.4$.

Analyzing in the same way the RBS data at room temperature [RT and RT(HCM) samples] results in the same damage efficiency independent of fluence, confirming again our assumption. This result suggests that the formed FP's are stable up to room temperature at least, this result being in agreement with the observation of Keinonen *et al.*[15] that the subsurface damage is recovered by annealing at a temperature around 500 K.

Interestingly enough, the above value of threshold energy, $E_t = 43$ eV, is not too far from the one advocated by Cerofolini *et al.*[18] to explain the damage production in

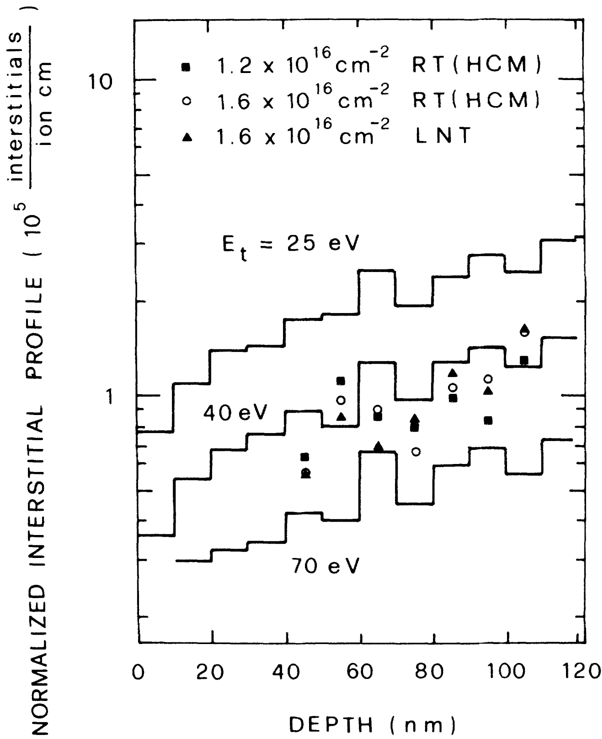

FIG. 8. Calculated (MARLOWE) vs measured (RBS) displaced atom profiles. MARLOWE calculations were carried out by taking the threshold energy for FP production as parameter and assuming that displaced atoms are only self-interstitials.

silicon by carbon implantation at 8.8 keV, as observed by Davies *et al.*[19] The reasons for such a high threshold energy are discussed in note 26 of Ref. 18.

This whole analysis leads us to conclude the following: (1) The damage efficiency is independent of the sample temperature (in the range 77–350 K) and implantation fluence (in the range 4×10^{15}–1.6×10^{16} cm^{-2}), (2) FP's are immobile and stable in silicon up to, at least, room temperature, and (3) the displacement field of the close FP is not the vectorial sum of the ones produced by the separated vacancy and self-interstitial, presumably because the positive stress due to the self-interstitial can be relieved punctually by the vacancy in its neighborhood.

B. Bulk region

Before considering the displacement field, we focus our attention on the various hydrogen configurations. Let C_* be the concentration of the molecular configuration H_* responsible for stress. This concentration is related to the total atomic concentration C_H,

$$C_H=[H]+2[H_2]+[\text{Si-H}]+\cdots ,$$

by the detailed way through which H_* is formed. For instance, if H_*=Si-H and all hydrogen atoms are in this configuration, then $C_*=C_H$; if $H_*=H_2$ and all hydrogen atoms are in this configuration, then $C_*=\frac{1}{2}C_H$; etc.

In the bulk region a strong nonlinear dependence of the RBS signal is observed as a function of the fluence (Fig. 2) and hence of hydrogen concentration. The XRD measurements show also a strong dependence of the static disorder u_0^{stat} on the hydrogen concentration for C_H high enough.

These facts are consistent with the following picture: the region where $C_* \ll \bar{C}$ is characterized by $C_* N_{\text{dis}}$ atoms displaced from their equilibrium positions arranged in C_* nonoverlapping displacement clouds, and the region where $C_* \gg \bar{C}$ is uniformly displaced with a local rms displacement $u_0(C_*)$. For any given H_* profile, the concentration $C_d^{H_*}$ of hydrogen-induced displaced silicon atoms ($C_d^{H_*}=[\text{Si}_d^{H_*}]$) is given by

$$C_d^{H_*}=N_{\text{dis}}C_* \quad \text{for } C_* \ll \bar{C}$$

and

$$C_d^{H_*}=n_{\text{Si}} \quad \text{for } C_* \gg \bar{C} .$$

This profile defines two space regions: The first region, $\{x:\ C_*(x) \ll \bar{C}\}$, is formed by an ordered lattice embedding $C_*(x)$ displacement clouds, each characterized by a local disorder with rms displacement u_0^{loc}; in the second region, $\{x:\ C_*(x) \gg \bar{C}\}$, all silicon atoms are assumed to be displaced from their lattice positions by an amount increasing as a power of C_*:

$$u_0(C_*)=u_0^{\text{loc}}+U_0[(C_*/\bar{C})^b-1] \quad \text{for } C_* > \bar{C} , \tag{2}$$

where U_0 and b are two suitable coefficients independent of the sample preparation (U_0 expresses the nonlinear contribution to the rms displacement) and the term -1 has been added to allow the continuity of $u_0(C_*)$ at $C_*=\bar{C}$. The sample preparation (target temperature, beam current, fluence, annealing temperature and duration) affects the fraction of C_H that forms the stressing species H_*:

$$C_*=C_H/k , \tag{3}$$

where k depends on the H_* structure and sample preparation (if H_* is formed by n hydrogen atoms and all hydrogen is in the H_* complex, then $k=n$); since the defect distribution presumably interferes with H_* formation, k is expected to be a function of depth, $k=k(x)$. Combining Eqs. (2) and (3), we get

$$u_0(C_H)=u_0^{\text{loc}}+U_0\left[\left[\frac{C_H}{k\bar{C}}\right]^b-1\right] \quad \text{for } C_H \gg k\bar{C}$$

$$\simeq U_0\left[\frac{C_H}{k\bar{C}}\right]^b$$

$$\text{for } C_H \gg k\bar{C}\max\left\{1,\ \left[\frac{u_0^{\text{loc}}}{U_0}\right]^{1/b}\right\} . \tag{4}$$

Interestingly enough, Eq. (4) shows that the concentration at which nonlinearity appears gives information on the structure of H_* (we shall return later to this point).

Of course, the implanted impurity is not the unique cause for strain and disorder. Indeed, vacancies, intersti-

tials, close FP's, and their clusters may as well be sources of displacement fields: It is well known that the interstitial produces a positive strain field, the vacancy a negative one (the amount of which is lower than that of the interstitial approximately by a factor of 20), and a cluster produces a displacement field whose nature depends on the cluster structure.[20] In our experimental situation the hydrogen implantation energy is not high enough to produce dense collisional cascades [amorphous islands are likely produced for transferred energy higher than approximately 5 keV;[21,18] divacancies require a transferred energy of about 2 keV (Ref. 15)] and TEM and HREM give no evidence for amorphous islands (extended defects are assumed to have a small effect on the overall disorder; their role will be considered later). Moreover, the transferred energy can produce only small vacancy-interstitial separation, so that we can reasonably consider only the close FP's with negligible displacement field.

The theoretical RBS can hence be calculated by combining the effect of close FP's with that of Si_d^H. To calculate the latter, the RBS version of MARLOWE is used to calculate the return probability of He^+ as a function of the self-interstitial concentration and of the root-mean-square displacement (Fig. 9). The following computational chain:

hydrogen profile $\rightarrow$ rms displacement profile

$\rightarrow He^+$ return probability

$\rightarrow$ equivalent interstitial profile

transforms the hydrogen profile into an equivalent interstitial profile. The analysis of the RBS spectrum in the fluence linear regime should give information on u_0^{loc}.

By contrast, since for small rms displacements u_0 the RBS yield of a uniformly displaced region increases as u_0^2

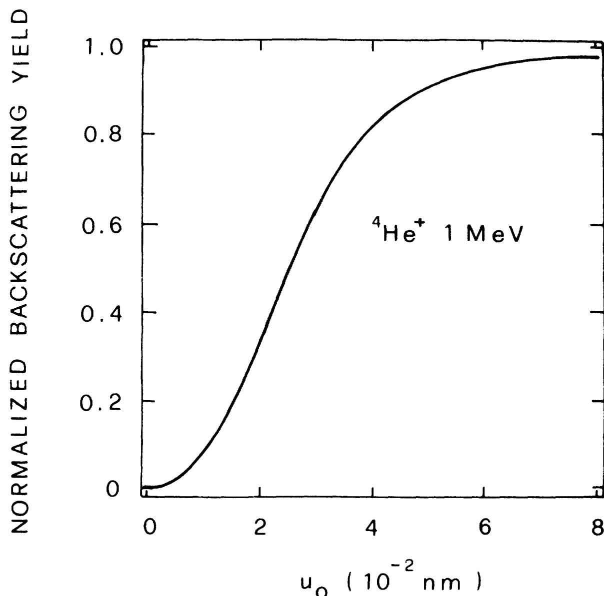

FIG. 9. Backscattering yield vs root-mean-square displacement for a uniformly displaced thick layer.

(Fig. 9), in the nonlinear regime the overall RBS signal I (corrected for the contributions of the virgin crystal, multiple scattering, and self-interstitials) should increase as

$$I \propto \int_{\{x:\ C_H > k\bar{C}\}} [u_0(x)]^2 dx = \int_{x_1(\Phi)}^{x_2(\Phi)} [u_0(x)]^2 dx \ , \quad (5)$$

where $x_1(\Phi)$ and $x_2(\Phi)$ are the roots of the equation

$$C_H(x) = k\bar{C} \quad (6)$$

and u_0 depends on x through $C_H(x)$.

If the hydrogen profile scales linearly with Φ (see, however, Ref. 6), i.e., if $C_H(x) = \Phi\eta(x)$, where the profile per unit fluence $\eta(x)$ is independent of Φ, inserting Eq. (4) into Eq. (5), we have

$$I \propto \Phi^{2b} \int_{x_1}^{x_2} [\eta(x)]^{2b} dx \ . \quad (7)$$

Since the profile $C_H(x)$ is in general very steep, for $C_H^{max} \gg k\bar{C}$ the roots of Eq. (6) depend very weakly on Φ, so that Eq. (7) gives $I \propto \Phi^{2b}$. (The implanted profile is typically of the kind

$$C_H(x) \approx (\Phi/\sqrt{2\pi}\sigma_p)\exp(-\{x-R_p\}^2/2\sigma_p^2) \ ,$$

so that

$$x = R_p \pm \sqrt{2}\sigma_p \ln^{1/2}(\sqrt{2\pi}\sigma_p k\bar{C}/\Phi) \ ,$$

which confirms the above statement.)

1. Linear regime

A preliminary analysis of the RBS in channeling of the virgin sample at 300 K gives $u_0^{th} = (6.6 \pm 0.3) \times 10^{-3}$ nm versus $u_0^{th} = 6.7 \times 10^{-3}$ nm, as calculated by Debye theory for a Debye temperature of 625 K; this agreement can be regarded as a validity proof of our RBS analysis procedure.

In the linear regime if $C_*(x)$ is known, the analysis of RBS spectra in the region where simultaneously $C_* \ll \bar{C}$ and no radiation damage is imparted to the crystal is actually able to furnish us with information on u_0^{loc}.

To show the procedure, we tentatively assume $C_* \approx C_H$ and observe that the RBS signal sees the contributions of $C_* N_{dis} \approx C_H N_{dis}$ silicon atoms per unit volume with rms displacement u_0^{loc} and of $n_{Si} - C_* N_{dis} \approx n_{Si} - C_H N_{dis}$ atoms per unit volume with rms thermal displacement u_0^{th}. Remembering that n_{Si} atoms per unit volume with rms displacement u_0^{th} are responsible for the virgin signal, from the channeling signal the contribution due to the local disorder inside single displacement clouds can be calculated. Assuming $N_{dis} = 10^3$, the rms displacement responsible for the observed RBS spectrum is $u_0^{loc} = (8.5 \pm 0.6) \times 10^{-3}$ nm, independent of Φ.

On another side, regarding the crystal as uniformly displaced with rms displacement given by

$$\langle u_0^2 \rangle \approx [(u_0^{loc})^2 C_H N_{dis} + (u_0^{th})^2 (n_{Si} - C_H N_{dis})]/n_{Si}$$
$$= (u_0^{th})^2 + [(u_0^{loc})^2 - (u_0^{th})^2] C_H N_{dis}/n_{Si}$$

and fitting the observed RBS spectra furnishes us with a value of $\langle u_0 \rangle$ and hence of $(u_0^{loc})^2 - (u_0^{th})^2$. Experimen-

tally we find

$$\Delta_0=[u_0^{\mathrm{loc}})^2-(u_0^{\mathrm{th}})^2]^{1/2}=(5.3\pm1.1)\times10^{-3}\text{ nm}\ .$$

The experimentally determined values of u_0^{loc} and Δ_0 satisfy well the composition rule $(u_0^{\mathrm{th}})^2+\Delta_0^2=(u_0^{\mathrm{loc}})^2$. This agreement can be regarded as a proof that the tentative values $N_{\mathrm{dis}}=10^3$ and $C_* \approx C_{\mathrm{H}}$ are not too far from reality.

2. Nonlinear regime

Extending the analysis to all RT(HCM) samples and correcting the measured RBS signals for the contributions of the virgin crystal, multiple scattering, and FP's (using the damage efficiency $y=2.3$), the signal I due to the hydrogen displacement field can be calculated. Two fluence regimes are clearly identified (Fig. 10): (1) the *low-fluence regime* ($\Phi<\overline{\Phi}$, with $\overline{\Phi}\simeq8\times10^{15}$ cm^{-2}), where $I\propto\Phi$, and (2) the *high-fluence regime* ($\Phi>\overline{\Phi}$), where I is no longer proportional to Φ and where eventually $I\propto\Phi^c$, with $c\simeq4$–5.

The first regime is explained by assuming that hydrogen (in some configuration not better specified in this moment) at low concentration introduces additional backscattering centers independent of one another.

The second regime is explained by assuming that in the high-fluence samples all atoms are displaced by an amount increasing as Φ^b, with $b\simeq2$. A more detailed, channel-by-channel analysis of this signal shows that it is primarily due to the region $\{x:\ x\gtrsim230\text{ nm}\}$, where no radiation damage is imparted to the crystal, and gives a more accurate specification of the relationship linking u_0 to C_{H}, $u_0\propto C_{\mathrm{H}}^{1.85}$. Remembering the composition law (1) and that u_0^{th} is independent of C_{H}, the above power law is consistent with the one obtained from XRD measurements, $u_0^{\mathrm{stat}}\propto C_{\mathrm{H}}^{2.25}$ (Sec. III A 2, item 2)— *two completely independent measurements give consistent relationships linking silicon root-mean-square displacement and hydrogen concentration.* A discrepancy is however noted: The perpendicular strain (as observed with multiple-crystal XRD) increases superlinearly with Φ for $\Phi\gtrsim10^{15}$ cm^{-2}; the rms displacement (as observed by RBS) increases superlinearly with Φ for $\Phi\gtrsim8\times10^{15}$ cm^{-2}.

The fluence at which the nonlinear behavior is observed in RBS measurements deserves a comment. Indeed, nonlinearities are expected to occur when the maximum concentration $C_*^{\max}$ of the stressing species H_* exceeds $n_{\mathrm{Si}}/N_{\mathrm{dis}}\simeq5\times10^{19}$–$10^{20}$ cm^{-3}; this value corresponds to different fluences $\overline{\Phi}$ in relation to the structure of H_* and to the process through which H_* is formed. A comparison of the predicted value of $\overline{\Phi}$ with the experimental one should therefore give information on the structure of H_*.

If H_* is a particular atomic configuration (e.g., the antibonding configuration observed by Picraux and Vook[22] in room-temperature ion implantation of deuterium at low energy, 13 keV, and relatively high fluence, 3×10^{15} cm^{-2}) and all hydrogen is in this configuration, one should have $\overline{\Phi}\simeq(1-2)\times10^{15}$ cm^{-2}. Actually, RBS gives evidence for a remarkably higher value of $\overline{\Phi}$ (Fig. 10) and shows that the RT sample does not contain the stressing species (Fig. 4).

If H_* is the H_2 molecular configuration and all hydrogen is in this configuration, then nonlinearities should occur at $\overline{\Phi}\simeq(2-4)\times10^{15}$ cm^{-2}. The comparison of this prediction with the value obtained from Fig. 10 ($\overline{\Phi}\simeq8\times10^{15}$ cm^{-2}) shows that either the stressing species contains more than two hydrogen atoms or only a part of the hydrogen atoms is in the H_2 molecular configuration.

Large clusters in the form of platelets directed along {111} direction, each containing approximately 350 atoms, have been observed in hydrogen-implanted silicon at approximately the same concentration as in this work.[3] We have given evidence for defects with the same habit planes and with approximately the same size [Fig. 3(b)]; moreover, we have also given evidence for hydrogen-related {100} defects [Fig 7(c)] and for {113} defects (not shown) related to self-interstitials.[23,24] However, the observed phenomenology cannot be ascribed to platelets because of the following reasons:

(1) If all hydrogen atoms were in the form of platelets, the characteristic fluence for superlinearity should be of the order 3×10^{17} cm^{-2}.

(2) The driving force for the formation of the stressing species is presumably a gain in the electronic energy (for instance, associated with the reaction $\mathrm{H}+\mathrm{H}\rightarrow\mathrm{H}_2$), which largely counterbalances the energy required to distort the lattice. The driving force towards the formation of extended defects ({001} or {111} platelets) should be a partial relief of the distortion energy. If this mechanism were important, however, it should be responsible for strain and disorder increasing with C_{H} more slowly than at low concentration where it does not act—u_0 and $\epsilon_\perp$

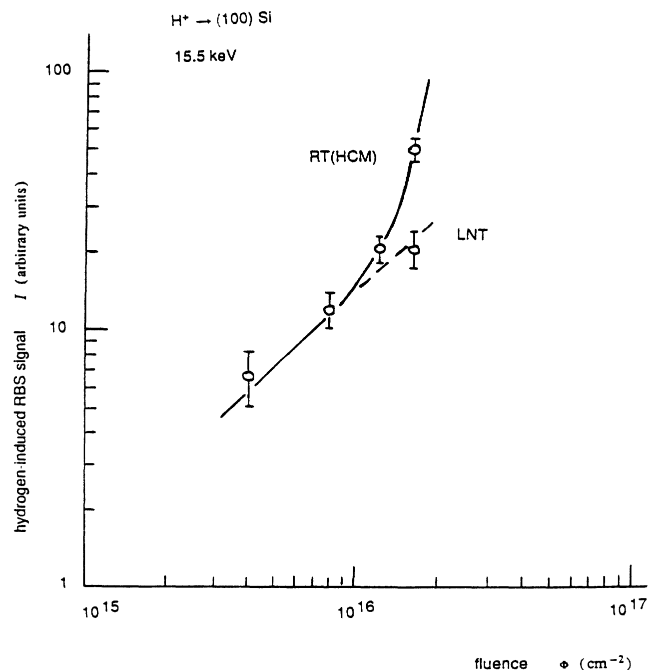

FIG. 10. RBS yield due to hydrogen vs implanted fluence. The lower is the implantation temperature; the higher is the fluence at which nonlinear phenomena appear.

should increase less than linearly with Φ. Since both u_0 and $\epsilon_\perp$ increase more than linearly with Φ, an important role of extended defects on the explanation of lattice disorder can be excluded.

We have hence undertaken a search by SIMS of H_2 as the most probable candidate for the stressing species. The profile of the H_2^+- to H^+-signal ratio as observed in an as-implanted RT(HCM) sample shows (Fig. 11) that H_2^+- to H^+-signal ratio is observed at very low concentration in the region where vacancies are produced (thus suggesting that nonstressing Si-H bonds are formed at vacancies) while H_2 is mainly formed in the damage-free region, however, associated with the RBS signal. Though this analysis is preliminary and purely qualitative (no attempt has been made to determine the absolute amounts of molecular hydrogen, which presumably has appreciable fragmentation during SIMS sputtering) and does not give any information either on the lattice location of stressing H_* or on the number of H_2 molecules present in H_* (the value of $\overline{\Phi}$ indicates that H_* is formed at most by 2–4 molecules), it however confirms that *the initial putative choice, $H_* = H_2$, seems at least reasonable.*

As a by-product, combining the profiles of Fig. 11 with the observation that the nonlinear contribution to the RBS signal comes mainly from the region $x > 230$ nm, we confirm that the parameter k in Eqs. (2) to (5) is a function of depth x.

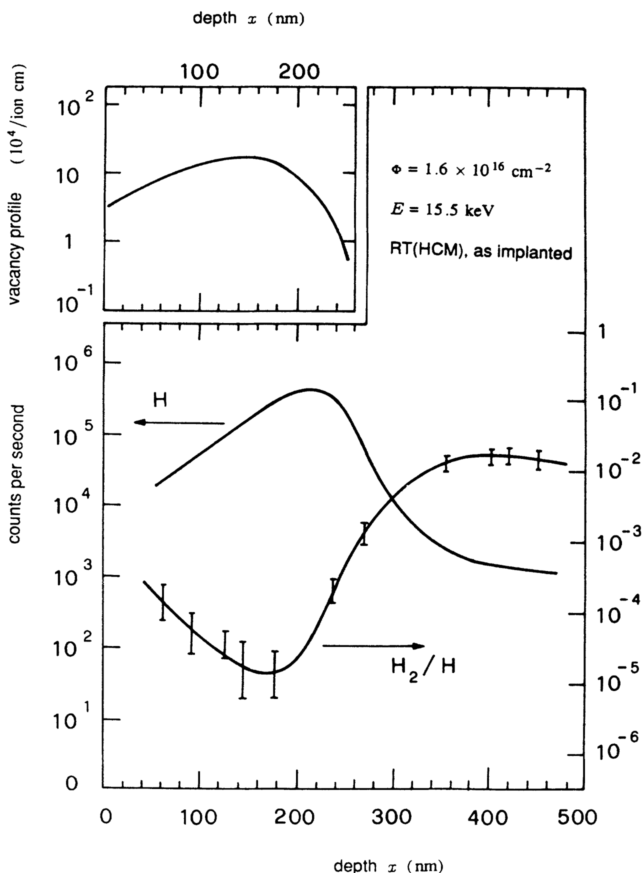

FIG. 11. SIMS evidence for molecular hydrogen in an as-implanted RT(HCM) sample ($\Phi = 1.6 \times 10^{16}$ cm^{-2}). In the region where vacancies are not present, the H_2^+- to H^+-signal ratio is higher than in the subsurface region by almost 2 orders of magnitude.

V. CONCLUSIONS

The previous description leads to the following conclusions.

(1) Close FP's are immobile in the crystal and stable up to the temperature of the RT(HCM) implantation (conservatively, FP's can be assumed to be stable up to 350 K); they produce a modest disorder and a negligible strain.

(2) At low implantation energy dense collisional cascades are not produced, but only close Frenkel pairs; the Frenkel-pair production yield at 15.5 keV is of about 2.3, independent of target temperature and beam current density, and consistent with a threshold energy of 43±5 eV.

(3) Since the implantation at high energy produces dense collisional cascades, *the accurate understanding of the physical phenomena occurring in ion implantation is only gained by low-energy experiments.*

(4) Hydrogen, when it is injected in atomic form, diffuses until bonded forms (such as Si-H and H_2) are produced; the H_2 molecular configuration is the source of a strong displacement field in the crystal.

(5) The hydrogen configuration responsible for the strong displacement field is formed with different efficiency in relation to depth, target temperature, and beam current density.

(6) The displacement field in the crystal can be increased by heating at temperature insufficiently high to produce appreciable hydrogen out-diffusion.

(7) The loss of hydrogen is responsible for a reduction of crystal disorder.

(8) *Neglecting the important role of the displacement field around the impurity may be a cause of serious discrepancies in the estimates of the threshold energy from experimental data.*

The validity of items in italic is not related to the specific system considered in this work.

In conclusion, the displacement field produced by low energy, high fluence, hydrogen implantation in silicon at room and liquid nitrogen temperature and its evolution after annealing in the range 400–800 °C have been studied experimentally by RBS, XRD, TEM, and HREM, and theoretically by MARLOWE simulation. The crystal disorder is strongly affected by the atomic or molecular state of hydrogen, this state being influenced by concentration and heat treatments. This conclusion throws a new light on the effect of the species on the damage centered on the projected range and often ascribed to FP's only.[21,18] Our study has also given evidence for seeming contradictions with previous experimental data on hydrogen-implanted silicon and germanium.[25,26] These discrepancies are removed by observing that in the previous studies the implantation energy was high enough to produce dense collisional cascades together with isolated FP's.[13]

*On leave from Department of Nuclear Engineering, Polytechnic of Milan, I-20133 Milan MI, Italy.

[1]L. Meda, G. F. Cerofolini, R. Dierckx, G. Mercurio, M. Servidori, F. Cembali, M. Anderle, R. Canteri, G. Ottaviani, C. Claeys, and J. Vanhellemont, Nucl. Instrum. Methods Phys. Res. Sect. B **39**, 381 (1989).

[2]S. J. Pearton, J. W. Corbett, and T. S. Shi, Appl. Phys. A **43**, 153 (1987).

[3]F. A. Ponce, M. N. Johnson, J. C. Tramontana, and J. Walker, Inst. Phys. Conf. Ser. **87**, 49 (1987).

[4]M. T. Robinson and I. M. Torrens, Phys. Rev. B **9**, 5008 (1974).

[5]J. B. Mitchell, J. A. Davies, L. M. Howe, R. S. Walker, K. B. Winterbon, G. Foti, and J. A. Moore, in *Ion Implantation in Semiconductors,* edited by S. Namba (Plenum, New York, 1975), p. 493.

[6]G. F. Cerofolini, L. Meda, C. Volpones, R. Dierckx, G. Mercurio, M. Anderle, R. Canteri, F. Cembali, R. Fabbri, and M. Servidori, Nucl. Instrum. Methods Phys. Res. Sect. B **39**, 26 (1989).

[7]C. W. Magee and E. M. Botnik, J. Vac. Sci. Technol. **19**, 47 (1981).

[8]J. Vanhellemont, H. Bender, and L. Rossou, Mat. Res. Soc. Symp. Proc. **115**, 247 (1988).

[9]F. Cembali, M. Servidori, and A. Zani, Solid-State Electron. **28**, 933 (1985).

[10]H. H. Andersen and J. F. Ziegler, *Hydrogen Stopping Powers and Ranges in All Elements* (Pergamon, New York, 1977).

[11]H. H. Andersen, Appl. Phys. **18**, 131 (1979).

[12]J. F. Ziegler, TRIM-89, *The Transport of Ions in Matter (Version 5.3),* March 7, 1989 (unpublished).

[13]The paradoxical behavior of the bulk peak at different implantation temperatures in relation to the expected behavior and to previous experimental evidence is discussed in G. F. Cerofolini and G. Ottaviani, Mater. Sci. Eng. B **4**, 19 (1989).

[14]W. K. Chu, R. H. Kastl, R. F. Lever, S. Mader, and B. J. Masters, Phys. Rev. B **16**, 3851 (1977).

[15]J. Keinonen, M. Hautala, E. Rauhala, V. Karttunen, A. Kuronen, J. Räisänen, J. Lahtinen, A. Vehanen, E. Punkka, and P. Hautojärvi, Phys. Rev. B **37**, 8269 (1988).

[16]G. F. Cerofolini and L. Meda, *Physical Chemistry of, in and on Silicon* (Springer-Verlag, Berlin, 1989).

[17]G. F. Cerofolini, in *Point and Extended Defects in Semiconductors,* edited by G. Benedek, A. Cavallini, and W. Schröter, (Plenum, New York, 1989), p. 123.

[18]G. F. Cerofolini, L. Meda, and C. Volpones, J. Appl. Phys. **63**, 4911 (1988).

[19]J. A. Davies, G. Foti, L. M. Howe, J. B. Mitchell, and K. Winterbon, Phys. Rev. Lett. **34**, 1141 (1975).

[20]M. Servidori, Nucl. Instrum. Methods Phys. Res. Sect. B **19/20**, 443 (1987).

[21]G. F. Cerofolini and L. Meda, Phys. Rev. B **36**, 5131 (1987).

[22]S. T. Picraux and F. L. Vook, Phys. Rev. B **18**, 2066 (1978). Though Picraux and Vook did not specify the beam current density of their experiment, this quantity is presumably of the same order as in our RT experiment. Extreme care must, however, be used when deuterium data are considered to simulate the behavior of hydrogen. Indeed, while the annealing kinetics are expected to be sensitive to isotope effects only, the released damages (and hence the defective structures of the target) in ^{1}H- and ^{2}H-implanted silicon differ remarkably. We have verified, both with numerical simulation (TRIM, Ref. 12) and with RBS analysis (data not shown, to be published elsewhere), that the distributions of the implanted deuterium and of displaced silicon at given energy are deeper than the corresponding distributions resulting after hydrogen implantation.

[23]J. Desseaux-Thibault, A. Bourret, and J. M. Peuisson, Inst. Phys. Conf. Ser. **67**, 71 (1983).

[24]G. F. Cerofolini, L. Meda, M. L. Polignano, G. Ottaviani, A. Armigliato, S. Solmi, H. Bender, and C. Claeys, in *Semiconductor Silicon 1986,* edited by H. R. Huff, T. Abe, and B. Kolbesen (The Electrochemical Society, Pennington, NJ, 1986), p. 706.

[25]J. B. Mitchell, G. Foti, L. M. Howe, J. A. Davies, S. U. Campisano, and E. Rimini, Radiat. Eff. **26**, 193 (1975).

[26]P. Baeri, S. U. Campisano, G. Foti, E. Rimini, and J. A. Davies, Appl. Phys. Lett. **26**, 424 (1975).

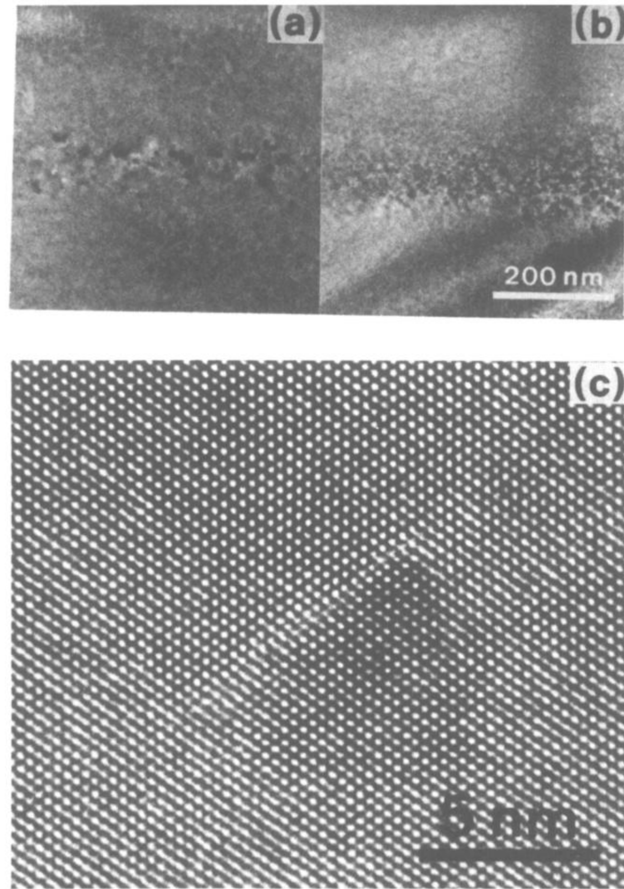

FIG. 3. (a) TEM cross section of the as-implanted RT(HCM) sample at $\Phi=4\times10^{15}$ cm^{-2}, (b) the same as (a) but with $\Phi=2\times10^{16}$ cm^{-2}, and (c) HREM image of part of sample (b) showing a (111) platelet similar to the ones observed by Ponce *et al.* (Ref. 3).

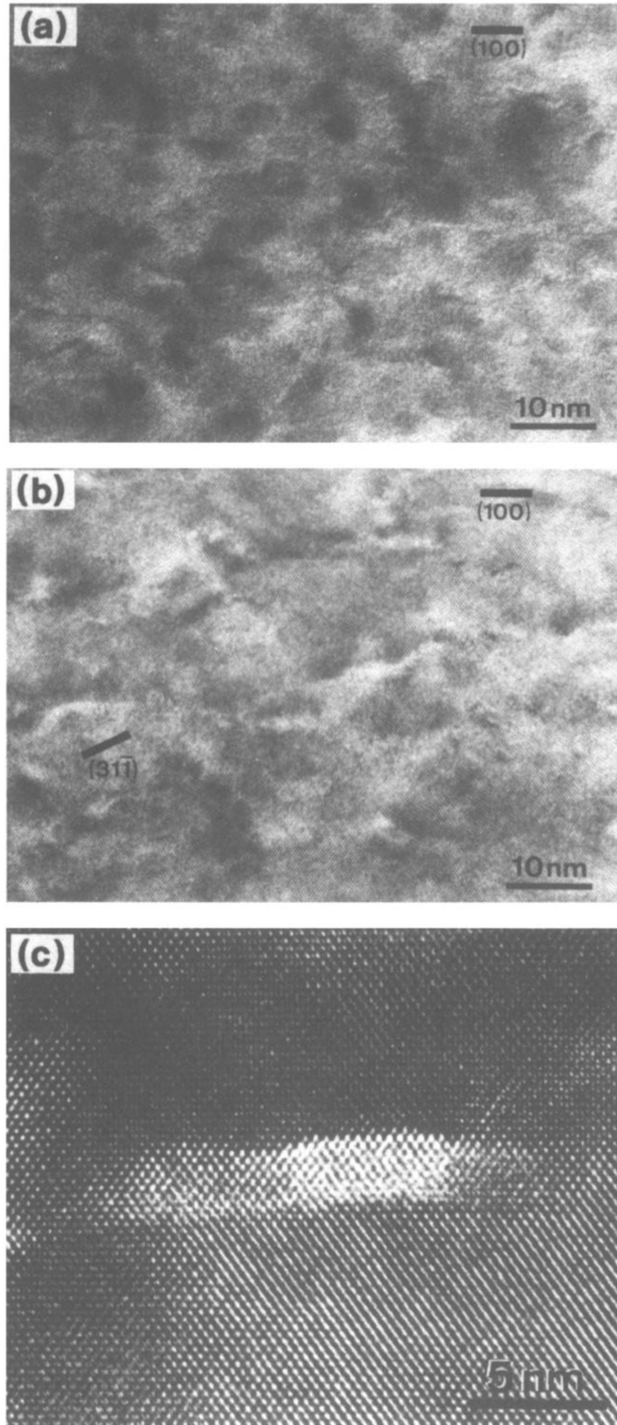

FIG. 7. (a) HREM cross section of an RT(HCM) as-implanted sample ($\Phi = 2\times10^{16}$ cm^{-2}). (b) Same sample annealed at 650 °C for 30 min. Coarsening of the defects is observed and the dominant habit planes are $\{113\}$ and $\{001\}$. (c) High voltage image of a (001) platelike defect.